PAPER

Check for updates

Study on the adsorption mechanism of benzoylurea insecticides onto modified hyperbranched polysilicon materials

Chaoran Liu,†[b] Xiaodong Huang,†[a] Zilin Meng,[b] Heng Qian,[b] Xinya Liu,[b] Runhua Lu,[b] Wenfeng Zhou, [b] Haixiang Gao [*b] and Donghui Xu [*a]

Several hyperbranched polysilicon (HBPS) materials with different end group modifications were designed and synthesized and the structures were characterized. The modified HBPS polymers were applied to the adsorption of benzoylurea insecticides (BUs). The binding mode and binding energy between the HBPS and BUs were quantified and the results of an adsorption kinetics study and an adsorption thermodynamics experiment were verified by calculation and mutual verification. The adsorption mechanism of BUs onto HBPS was also discussed. The theoretical results show that the most effective way to combine the adsorbent and BUs is *via* hydrogen bonding when the end group is an amino group. Moreover, the most effective combination when the end group is β-cyclodextrin is the interaction of the BUs with the interior of the cavity to form a host–guest coating. The theoretical results of other end group-modified HBPS materials were also obtained and verified by adsorption experiments. In this work, an experimental method for obtaining the binding mode by theoretical calculations and then verifying it according to adsorption experiments was established.

1. Introduction

Benzoylurea insecticides (BUs) are a class of pesticides that interfere with the formation of chitin in insect cuticles, which will block molting and lead to subsequent rupture of the malformed cuticle or death from starvation.[1,2] After several decades of development, these insecticides are still widely used in agriculture. BUs, such as diflubenzuron, hexaflumuron, flufenoxuron, teflubenzuron, lufenuron and chlorfluazuron, have been widely used in pest management systems due to their attractive properties, which include high insecticidal activity, great selectivity and rapid biodegradation.[3] The high employment of these insecticides has led to the accumulation of their residues in soil, groundwater and surface water. According to European Union regulations, the content of BUs residues in environmental water must be less than 0.05 mg kg^{-1}.[4] Some sensitive analytical methods for monitoring these compounds were developed. However, there are few reports on the adsorption mechanism of BUs.

Hyperbranched polysilicon (HBPS) materials have high application value in the fields of flame retardant materials, drug loading and material modification due to their good chemical stability, good material compatibility and their high number of reactive functional end groups.[5,6] In previous work, the application of a β-cyclodextrin (β-CD)-modified and amino-modified HBPS material in the analytical detection of BUs residues demonstrates its potential as an adsorbent material.[7,8] At the same time, the material compatibility and end group activity of HBPS materials are also promising. The end group modification of the HBPS material can further utilize its highly branched spatial structure, increase the number of surface active groups per unit material and expand its application range.[9,10]

Density functional theory (DFT) is a representation of quantum theory developed in 1964 based on the Thomas–Femi model and proposed in the Hohenberg–Kohn theorem.[11,12] In recent years, DFT has been combined with molecular dynamics methods. Many new developments have become an important foundation and technical core for the calculation of condensed matter physics, computational materials science and computational quantum chemistry. Quantum chemical calculations have been gradually applied to study the adsorption and diffusion behavior of adsorbed materials on target analytes.[13] Through quantum chemical methods, the interaction between particles is calculated to obtain adsorbed materials and target compounds in different substrates (gaseous or liquid). The density functionalization plus attenuation dispersion proposed by Wu describes the hydrogen peroxide and hydroquinone systems,[14] indicating that the theory can be applied to water, surface physical adsorption and chemical reactions involving

[a]*Institute of Vegetables and Flowers, Chinese Academy of Agricultural Sciences, Key Laboratory of Vegetables Quality and Safety Control, Ministry of Agriculture and Rural Affairs of China, Beijing 100081, China. E-mail: xudonghui@caas.cn*

[b]*Department of Applied Chemistry, College of Science, China Agricultural University, Beijing 100193, China. E-mail: hxgao@cau.edu.cn*

† Chaoran Liu and Xiaodong Huang contributed equally to this work.

hydrogen bonding. Mueller *et al.* used DFT, PBE exchange-related functional theory and periodic boundary conditions to study the adsorption of hydrogen molecules in the material by simulating the combination of the spatial configuration of metal–organic frameworks and hydrogen molecules.[15] However, there have been few reports on the study of mechanisms using quantum chemical calculation methods in solid phase extraction adsorption.[16] Since the HBPS material has the characteristics of strong plasticity and easy modification,[17] the combination of the adsorbent and the target analyte and the spatial configuration after the combination are simulated by the quantum chemical calculation method, and then the macroscopic adsorption test is carried out to verify the calculation results.

In this study, a series of HBPS adsorbents with different end groups were designed and synthesized.[18,19] The adsorption mechanism between different end group-modified HBPS materials and BUs was discussed by measuring the adsorption kinetics, adsorption isotherms and adsorption binding energy. The binding mechanism of the modified HBPS to the target analyte and the molecular structure of the adsorbed material and the target analyte were optimized by quantum chemical calculations. The combination method and binding energy were optimized, and the calculation results were confirmed by the experimental results. The binding mechanism between the adsorption materials of different end groups and the target analytes was discussed. The results were verified by the results of molecular simulation to prove the feasibility of the proposed method. This method provides predictability and diverse possibilities for studying the extraction mechanism of target analytes and guiding the molecular design and synthesis of new, selective adsorbents.

2. Materials and methods

2.1 Chemicals and reagents

Stock standard solutions of individual compounds (diflubenzuron, hexaflumuron, flufenoxuron, teflubenzuron, lufenuron, and chlorfluazuron) at a concentration of 1000 mg L^{-1} were prepared by exact weighing of the powder that was then dissolved in methanol or acetonitrile. A working standard mixture at a concentration of 10 mg L^{-1} was prepared in acetonitrile by appropriate dilutions of the stock solutions. All solutions were stored at -18 °C in the dark.

The pesticide standards (diflubenzuron, hexaflumuron, flufenoxuron, teflubenzuron, lufenuron, and chlorfluazuron) were purchased from Aladdin Reagent Corporation (Shanghai, China). Ammonia solution, ethanol and acetone were purchased from Beijing Chemical Factory (Beijing, China).

2.2 Instrumentation

Chromatographic analysis was performed on an Agilent 1260 HPLC (Quantum Design, San Diego, CA, USA) system equipped with an ultraviolet detector (UVD) and an autosampler. Sample separations were conducted on a Venusil XBP C18 (L) column (250 × 4.6 mm i.d., 5 μm) with a Spursil C18 guard column

(10 × 2.1 mm i.d., 5 μm). A mixture of methanol (A) and water (B) was used as the mobile phase at a flow rate of 0.7 mL min^{-1}. The gradient conditions were 79% A and 21% B for 2 min, then increased from 79% A to 89% A over 21 min and decreased from 89% A to 79% A.

2.3 Synthesis of terminally modified HBPS materials

2.3.1 Synthesis of amino-modified HBPS. First, 0.5 g cetyltrimethylammonium bromide was added to 70 mL deionized water. Then, 5 mL ethanol, 15 mL diethyl ether and 0.8 mL 30% aqueous ammonia were added. The mixture was stirred at 40 °C for 30 min. Then, 2.5 mL tetraethyl orthosilicate and 0.1 mL triaminopropyltriethoxysilane were mixed and added to the above liquid and stirred at 40 °C for 4 h. At the end of the reaction, hydrochloric acid was added to terminate the reaction, and the mixture was centrifuged at 3500 rpm for 5 min. The precipitate was transferred to the sediment at the bottom and dried under vacuum at 50 °C for 8 h.[20]

2.3.2 Synthesis of carboxyl-modified HBPS. First, 0.5 g amino-modified HBPS was added to 50 mL DMF. Then, 4.5 g succinic anhydride was dissolved in 12.5 mL of DMF and added to 4.5 mL triethanolamine. After a 30 min reaction, the obtained product was washed with water and ethanol and dried under vacuum at 50 °C for 8 h.

2.3.3 Synthesis of phenyl-modified HBPS. Briefly, 35 mg 1-(3-dimethylaminopropyl)-3-ethylcarbodiimide hydrochloride (EDC), 20 mg *N*-hydroxysuccinimide (NHS) and 30 mg carboxyl-modified HBPS was added to 20 mL DMF, sonicated for 5 min and stirred at 35 °C for 30 min. Then, 200 μL benzylamine was added to 1 mL of ethanol and the above reaction solution was added and stirred at 35 °C for 5 h. The obtained product was washed with water and ethanol and then dried under vacuum at 50 °C for 8 h.

2.3.4 Synthesis of alkyl-modified HBPS. First, 35 mg EDC, 20 mg NHS and 30 mg carboxyl-modified HBPS was added to 20 mL DMF, sonicated for 5 min and stirred at 35 °C for 30 min. Then, 200 μL hexylamine was added to 1 mL ethanol and the above reaction solution was added dropwise and stirred at 35 °C for 5 h. After suction filtration under reduced pressure, the obtained product was washed with water and ethanol and then dried under vacuum at 50 °C for 8 h.

2.3.5 Synthesis of β-CD-modified HBPS

2.3.5.1 Synthesis of mono-6-deoxy-(p-toluenesulfonyl)-β-CD (β-CD-O-Ts). NaOH (2.4 g) was dissolved in 8 mL water. Then, 22.7 g β-CD and 200 mL water were added to the solution, and the mixture was stirred at 10–15 °C for 15 min. *p*-Toluenesulfonyl chloride (5.76 g) was dissolved in 12 mL acetonitrile, added dropwise to the above reaction solution and stirred at 12–13 °C for 4 h. 1 mL hydrochloric acid was added to terminate the reaction. The precipitate was obtained by suction filtration under reduced pressure and dried under vacuum at 50 °C for 8 h.

2.3.5.2 Synthesis of β-CD-modified HBPS. First, 0.5 g β-CD-O-Ts was added to 50 mL DMF under stirring. Then, 1.5 g amino-modified HBPS was slowly added, and 5 drops of triethylamine were added and reacted at 140 °C for 24 h. After suction

filtration under reduced pressure, the obtained product was washed with water and acetone and then dried at 50 °C for 8 h.

2.4 Computational model and method for DFT research

In this study, the geometrical model of six kinds of end-modified HBPS materials was constructed by DFT. Then, all the atoms in the model were fixed with water set as the solvent and one was added at different initial positions. Similarly, the destructive urea molecule of the geometric structure model was constructed and the diflubenzuron molecule could move freely in the solvent space. After the geometric configuration optimization calculation, the stable configuration with the lowest energy at different positions of different adsorbent materials was obtained. From the optimal adsorption configuration obtained after optimization, the adsorption energy of diflubenzuron was calculated. The effective adsorption position of diflubenzuron and adsorbent was distinguished according to the size of adsorption energy, and the microstructure of each adsorption configuration was investigated. The effect of different functional groups in the end group-modified HBPS materials on the adsorption energy of diflubenzuron was evaluated.[21]

According to the characteristics of the material and the possible adsorption mechanism, in the case determined by the calculation method B3LYP, the basis set of 6-31G (d,p) was selected to improve the calculation accuracy. After calculation and optimization, the binding energy of the corresponding optimal position of diflubenzuron and the different end group-modified HBPS material binding configurations were obtained the different end group-modified HBPS and diflubenzuron were subtracted. The sum of the energy of the geometric configuration gave the binding energy of diflubenzuron and HBPS adsorption, which was expressed by the following formula:

$$\Delta E_{ads} = E_{HBPS-BU} - E_{HBPS} - E_{BU} \tag{1}$$

where $E_{HBPS-BU}$ represents the energy of the HBPS material in the stable configuration of diflubenzuron and E_{HBPS} and E_{BU} represent the energy of the HBPS and diflubenzuron geometry, respectively. By comparing the energy of different positions and bonding after optimization, the relative stability of adsorption, the preferential position and the configuration of adsorption can be obtained.

2.5 Adsorption studies

Adsorption studies for the evaluation of the adsorption of BUs from aqueous solutions onto the adsorbent were carried out in triplicate. Typically, 3.0 mg of adsorbent was dispersed in a conical flask with 30 mL of a dye solution (60–120 mg L^{-1}). The conical flask was shaken by an oscillator (SHA-BA, Changzhou HUAO Instrument Co., China) for 6 h at a speed of 150 rpm and at the temperatures of 30 °C. The adsorptive precipitations were separated from the dye solution by an adscititious magnet.[22]

The concentrations of the supernatant containing residual BUs were determined by HPLC-UV. The amount of BUs

adsorbed on adsorbent per unit mass, at equilibrium, q_e (mg g^{-1}), and at any time t, q_t (mg g^{-1}), was calculated by eqn (2) and (3), respectively. The BU percent adsorption was calculated using eqn (4).

$$q_e = \frac{(C_0 - C_e)V}{m} \tag{2}$$

$$q_t = \frac{(C_0 - C_t)V}{m} \tag{3}$$

$$\text{Adsorption\%} = \frac{C_0 - C_e}{C_0} \times 100 \tag{4}$$

where C_0 (mg L^{-1}) is the initial BU concentration; C_e (mg L^{-1}) is the BU concentration at equilibrium; C_t (mg L^{-1}) is the BU concentration at time t (min); V (L) is the volume of the solution and m (g) is the mass of the adsorbent used.

3. Results and discussion

3.1 Characterization of end-modified HBPS

The infrared spectrum of the terminal-modified HBPS is shown in Fig. 1. The main characteristic peak of the HBPS material is the characteristic absorption peak of the Si–O bond at approximately 1045 cm^{-1}, which exists in all end group-modified HBPS materials and proves that all of the materials are HBPS. For the hyperbranched polymer in which the terminal group is an amino group, there is an absorption peak of a C=O double bond at 1656 cm^{-1}, which is a characteristic peak generated by the amide bond formed during the modification. For the hyperbranched polymer whose terminal group was modified with a carboxyl group, the broad peak at 3030–3600 cm^{-1} is the characteristic absorption peak of the hydroxyl group in the carboxyl group; in the phenyl-modified HBPS material, the characteristic absorption of the Si–O bond is very strong, which masks the characteristic absorption of the benzene ring at

Fig. 1 FT-IR spectral characterization of HBPS-NH$_2$, HBPS-Ph, HBPS-β-CD, HBPS-C$_6$H$_{13}$ and HBPS-COOH.

1040 cm^{-1}, but the infrared spectrum of this compound is different from the infrared spectra of the other products, as it has no hydrogen bond peak generated by surface active hydrogen atoms; when the hyperbranched end group is a hexyl chain, the polymer has a characteristic absorption peak of methylene at 2920 cm^{-1} and 2850 cm^{-1}, while the HBPS with a β-CD end group has a strong hydroxyl absorption peak and sub-methyl absorption peak.[23]

The SEM and TEM images are shown in Fig. 2. The TEM images of HBPS exhibits a distinct core–shell structure and many folds exist on the surface of the spherical structure, which increase the specific surface area.[24] For the SEM images of the end-modified HBPS materials, the surfaces become denser and smoother with the introduction of the end group modifications, and the rough surfaces are still retained.[25,26]
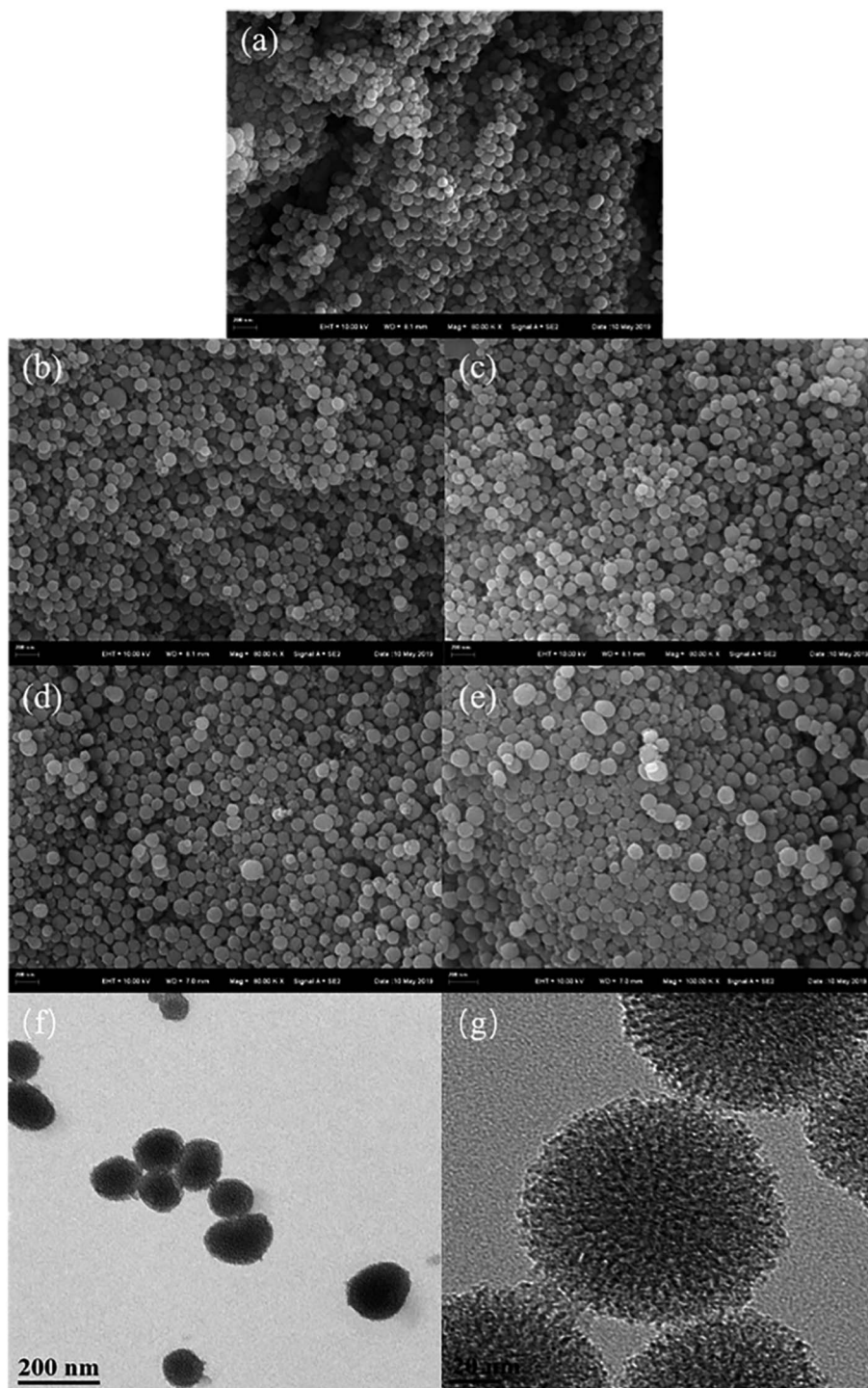

Fig. 2 SEM images of HBPS-NH$_2$ (a), HBPS-Ph (b), HBPS-COOH (c), HBPS-C$_6$H$_{13}$ (d) and HBPS-β-CD (e) and TEM images of HBPS (f and g).
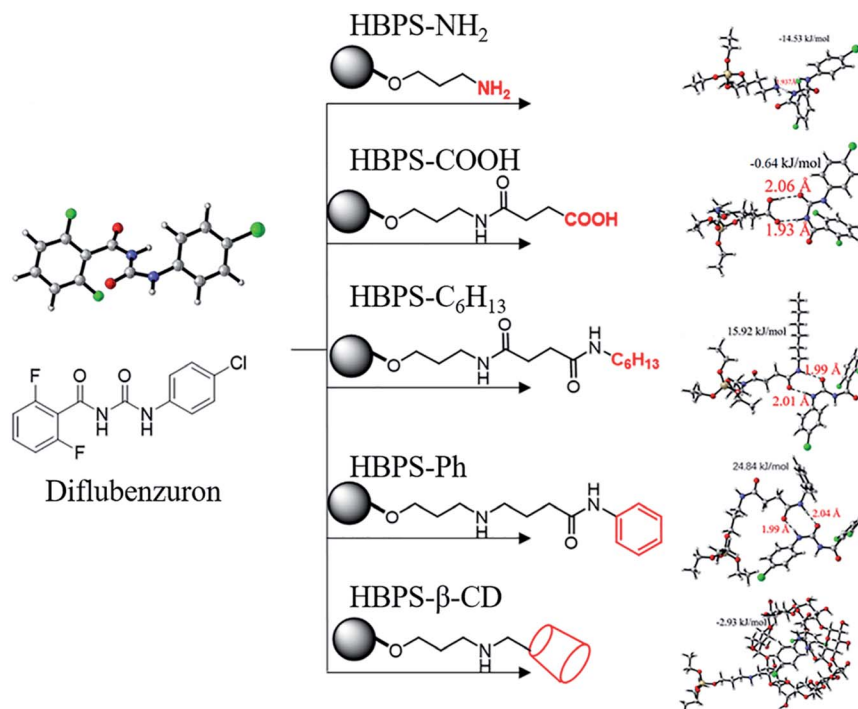
Fig. 3 Binding mode and binding energy between modified HBPS and diflubenzuron.

3.2 DFT calculation study

According to the calculation method described above, the geometric configurations of the six end group-modified HBPS materials and diflubenzuron molecules were calculated. Fig. 3 shows the combination of the diflubenzuron and the terminal-modified HBPS materials and the bond length. For the HBPS material whose terminal group is an amino group, the main part of the hyperbranched structure has a limited effect on the adsorption bonding and the main position of adsorption is the hydrogen bond of the amino group.[27,28] Other HBPS materials can form a 6- or 8-membered ring structure by hydrogen bonding with the acyl urea skeleton in diflubenzuron due to its amide bond, so it is used as one of the main positions of adsorption simulation.[29] The π–π interaction in which the

phenyl group may exist. The host–guest interaction in which the terminal group is β-CD, and the carboxyl group in the terminal group are preferentially calculated. It can be seen from Fig. 3 that the HBPS material whose terminal group is an amino group, a carboxyl group, phenyl group or hexyl group is combined with diflubenzuron mainly by hydrogen bonding. When the amide bond is combined with the acyl urea skeleton in diflubenzuron to form a cyclic structure, the energy is minimal, especially in the combination with the hyperbranched silicone having a terminal phenyl groups and the expected mutual π–π interactions.[30,31] The effect did not form a stable configuration. In the binding structure of HBPS with β-CD and diflubenzuron, due to hydrophobic interactions, the diflubenzuron molecule enters the internal hydrophobic cavity of β-

Table 1 Binding energy between diflubenzuron and modified HBPS in aqueous solvent

Model	Correction value	G (Hartree)	ΔG (kcal mol^{-1})	ΔG (kJ mol^{-1})
Diflubenzuron	0.1602	−1458.26		
HBPS-NH$_2$	0.2790	−1001.56		
HBPS-COOH	0.3471	−1381.94		
HBPS-C$_6$H$_{13}$	0.5172	−1597.64		
HBPS-β-CD	1.3850	−5198.26		
HBPS-Ph	0.4587	−1632.16		
Diflubenzuron–HBPS-NH$_2$	0.4586	−2459.83	−3.4753	−14.5335
Diflubenzuron–HBPS-COOH	0.5269	−2840.21	−0.1546	−0.6464
Diflubenzuron–HBPS-C$_6$H$_{13}$	0.7007	−3055.89	3.8065	15.9186
Diflubenzuron–HBPS-β-CD	1.5728	−6656.52	−0.7012	−2.9323
Diflubenzuron–HBPS-Ph	0.6461	−3090.42	5.9395	24.8390

CD to form host–guest interactions. The situation and the combined Gibbs free energy indicate that the probability of this happening is high. The calculation results of the specific Gibbs free energy and its variation values are shown in Table 1. The mode of action and results of other BUs and terminal-modified HBPS are similar to the simulation results of diflubenzuron and are not listed.

3.3 Effect of initial concentration and adsorption time on the adsorption of BUs

The initial concentration and adsorption time of the target analyte in the sample solution have an important influence on the adsorption process and adsorption mechanism.[32] Therefore, in the presence of different target analytes and different initial concentrations in the solution, the adsorption rate changes with the adsorption time. The experimental results are shown in Fig. 3. Taking dipyridamole as an example, when the

initial concentration of the terminal amino group-modified HBPS material is 120 mg L^{-1}, the adsorbent adsorbs the target analyte after 1 h. The adsorption rate was 85.6%, and the adsorption rate reached 92.1% at 3 h, after which the adsorption tended to plateau. At the initial concentration of 100 mg L^{-1}, the adsorption rates at 1 h and 3 h were 83.8% and 91.1%, respectively. Other target analyte adsorption rates vary with time and initial concentration. The experimental results show that at the beginning of adsorption, the terminal amino HBPS adsorbent rapidly adsorbs the BUs and then approaches equilibrium and the active adsorption of the target analyte onto the adsorbent in the process. The sites are then combined. After a period of time, the adsorption sites on the surface of the adsorbent are reduced, and adsorption of target analyte becomes difficult, leading to an adsorption plateau. The adsorption results of six BUs onto amino-modified HBPS are shown in Fig. 4.
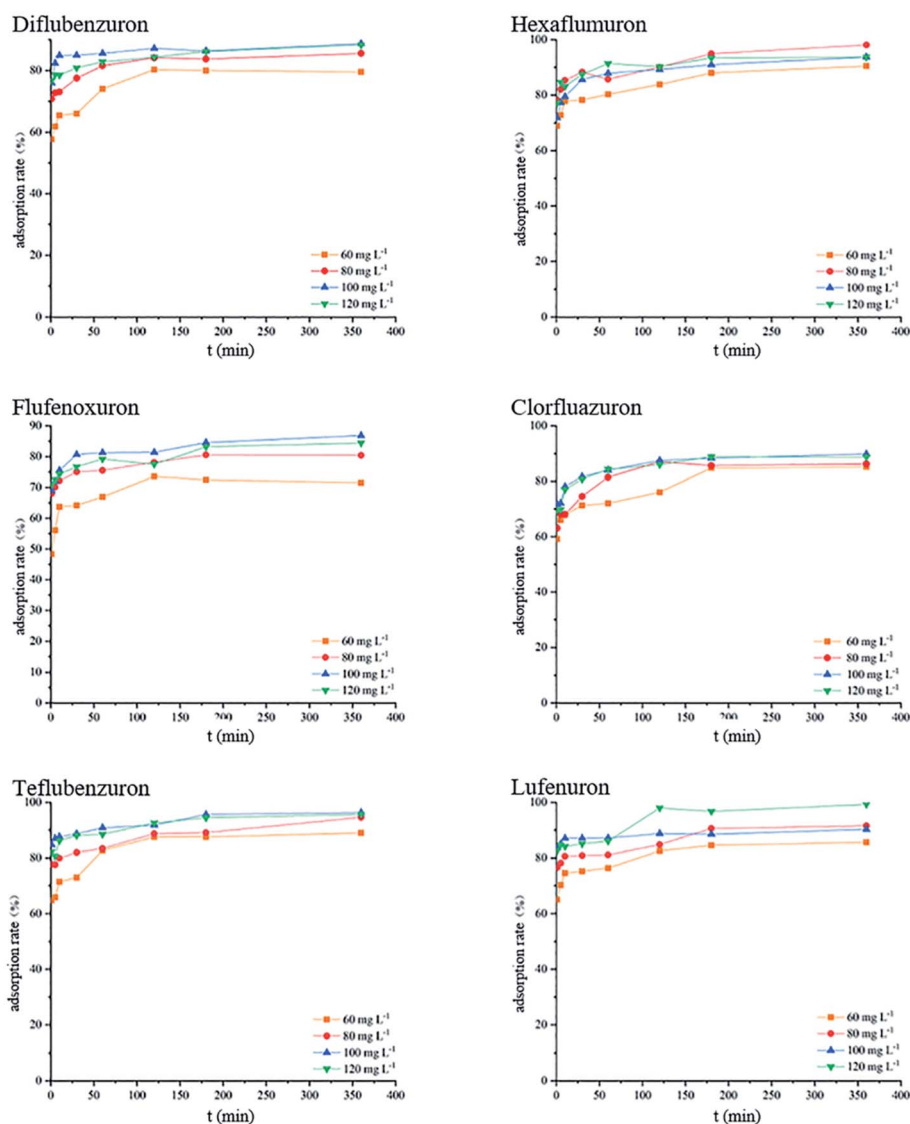

Fig. 4 The adsorption rate of each analyte at different times.

Table 2 Adsorption kinetics constants for diflubenzuron adsorption on HBPS-NH$_2$ for different initial concentrations

C_0 (mg L^{-1})	$q_{e,exp}$ (mg g^{-1})	Pseudo-first order kinetic model			Pseudo-second order kinetic model		
		$q_{e,cal}$ (mg g^{-1})	k_1 (min^{-1})	R^2	$q_{e,cal}$ (mg g^{-1})	k_2 (g mg^{-1} min^{-1})	R^2
60	153.29	34.36	0.0223	0.8557	156.35	0.0412	0.9998
80	152.23	49.47	0.0215	0.9393	158.16	0.0310	0.9999
100	159.31	56.16	0.0089	0.8918	160.83	0.0044	0.9995
120	160.12	82.41	0.0070	0.8137	161.73	0.0031	1.0000

Table 3 Adsorption kinetics constants for diflubenzuron adsorption on HBPS-COOH for different initial concentrations

C_0 (mg L^{-1})	$q_{e,exp}$ (mg g^{-1})	Pseudo-first order kinetic model			Pseudo-second order kinetic model		
		$q_{e,cal}$ (mg g^{-1})	k_1 (min^{-1})	R^2	$q_{e,cal}$ (mg g^{-1})	k_2 (g mg^{-1} min^{-1})	R^2
60	93.74	26.15	0.0287	0.7315	94.16	0.0329	0.9999
80	97.66	34.12	0.0253	0.6834	96.41	0.0348	1.0000
100	98.16	42.92	0.0084	0.8352	98.07	0.0047	0.9993
120	99.48	47.15	0.0075	0.7517	100.09	0.0048	0.9995

3.4 Adsorption kinetics

For further study of the adsorption kinetics, the classical adsorption model (pseudo-first order kinetic model and pseudo-second order kinetic model) were applied to simulate the adsorption kinetics of benzoylureas and the adsorbent. The formula is:

$$\log(q_e - q_t) = \log q_e - \frac{k_1 t}{2.303} \quad (5)$$

$$\frac{t}{q_t} = \frac{1}{k_2 q_e^2} + \frac{1}{q} t \quad (6)$$

where q_e (mg^{-1}) and q_t (mg^{-1}) are the amount of target compound adsorbed at equilibrium time and time t (min). k_1 is the rate constant of the pseudo-first order kinetic model. k_2 is the rate constant (mg g^{-1} min^{-1}) of the pseudo-second order kinetic model.

The calculated dynamic parameters are shown in the Tables 2–6. The linear correlation coefficient $R^2 \geq 0.999$ for the pseudo-second order kinetic model. The results of $q_{e,cal}$ and $q_{e,exp}$ calculated by the pseudo-second order kinetic model are in good agreement with the experimental data. Therefore, by comparing the calculated values of the two models with the experimental values obtained in the experiment, it can be seen that the adsorption process of magnetic hyperbranched polyester adsorbent for benzoylurea compounds conforms to the pseudo-second order kinetic model, indicating that the adsorption mechanism mainly depends on the interaction between the adsorbent and the target analyte.

3.5 Adsorption isotherms

Isotherm studies can highlight the adsorptive characteristics of an adsorbent, which is the most important parameter for the design of adsorption processes. In this work, the two well-known Langmuir and Freundlich isotherm models were applied to determine the equilibrium adsorption of BUs on the adsorbent.

The Langmuir adsorption isotherm can be represented as follows:

$$\frac{C_e}{q_e} = \frac{1}{K_L q_{max}} + \frac{C_e}{q_{max}} \quad (7)$$

where C_e (mg L^{-1}) is the BU equilibrium concentration in the solution; q_e (mg g^{-1}) is the amount of BUs adsorbed at equilibrium; q_{max} (mg g^{-1}) is the maximum theoretical adsorption capacity and K_L (L mg^{-1}) is the Langmuir adsorption constant

Table 4 Adsorption kinetics constants for diflubenzuron adsorption on HBPS-C$_6$H$_{14}$ for different initial concentrations

C_0 (mg L^{-1})	$q_{e,exp}$ (mg g^{-1})	Pseudo-first order kinetic model			Pseudo-second order kinetic model		
		$q_{e,cal}$ (mg g^{-1})	k_1 (min^{-1})	R^2	$q_{e,cal}$ (mg g^{-1})	k_2 (g mg^{-1} min^{-1})	R^2
60	77.21	24.25	0.0308	0.7182	78.31	0.0410	0.9998
80	84.16	37.09	0.0216	0.7401	84.23	0.0382	0.9998
100	86.92	37.74	0.0090	0.8222	85.82	0.0044	0.9997
120	87.62	44.96	0.0064	0.6958	87.55	0.0042	0.9994

Table 5 Adsorption kinetics constants for diflubenzuron adsorption on HBPS-β-CD for different initial concentrations

C_0 (mg L^{-1})	$q_{e,exp}$ (mg g^{-1})	Pseudo-first order kinetic model			Pseudo-second order kinetic model		
		$q_{e,cal}$ (mg g^{-1})	k_1 (min^{-1})	R^2	$q_{e,cal}$ (mg g^{-1})	k_2 (g mg^{-1} min^{-1})	R^2
60	114.25	44.58	0.0269	0.8756	114.76	0.0278	0.9992
80	118.42	52.65	0.0244	0.8319	117.15	0.0350	1.0000
100	121.46	57.52	0.0083	0.8488	123.19	0.0048	0.9997
120	126.83	64.62	0.0065	0.7368	127.07	0.0040	0.9999

Table 6 Adsorption kinetics constants for diflubenzuron adsorption on HBPS-Ph for different initial concentrations

C_0 (mg L^{-1})	$q_{e,exp}$ (mg g^{-1})	Pseudo-first order kinetic model			Pseudo-second order kinetic model		
		$q_{e,cal}$ (mg g^{-1})	k_1 (min^{-1})	R^2	$q_{e,cal}$ (mg g^{-1})	k_2 (g mg^{-1} min^{-1})	R^2
60	91.05	34.54	0.0209	0.7024	92.12	0.0317	0.9999
80	94.39	42.53	0.0220	0.7451	96.35	0.0415	0.9999
100	98.07	47.34	0.0089	0.8668	99.63	0.0048	0.9997
120	101.62	54.85	0.0090	0.9173	101.42	0.0032	0.9993

related to the heat of adsorption. The slope and intercept of linear plots of C_e/q_e versus C_e yield the values of $1/q_{max}$ and $1/K_L q_{max}$, respectively.

The linearized form of the Freundlich isotherm can be given as follows:

$$\log q_e = \log K_F + \frac{q}{n} \log C_e \qquad (8)$$

where K_F (mg$^{1-1/n}$ L$^{1/n}$ g^{-1}) is related to the adsorption capacity of the adsorbent and $1/n$ is a constant depicting the adsorption

intensity. The slope and intercept of linear plots of $\log q_e$ versus $\log C_e$ yield the values of $1/n$ and $\log K_F$, respectively.

According to Langmuir theory, it assumes that adsorption occurs at a specific homogeneous site within the adsorbent. All sites are equivalent and there are no interactions between adsorbate molecules. The Freundlich isotherm is employed to describe heterogeneous systems and reversible adsorption, which is not restricted to monolayer formations.

The equilibrium adsorption isotherms of the BUs on the adsorbent were carried out at 30 °C, as shown in Fig. 3. Tables

Table 7 Adsorption isotherm constants for BUs adsorption on HBPS-NH$_2$

T = 303 K	Langmuir isotherm model				Freundlich isotherm model		
	q_{max} (mg g^{-1})	K_L	R^2	R_L	K_F (mg$^{1-1/n}$ L$^{1/n}$ g^{-1})	n	R^2
Diflubenzuron	160.13	0.932	0.9910	0–1	88.185	4.0447	0.8146
Hexaflumuron	151.72	1.048	0.9945	0–1	81.502	4.5144	0.8887
Flufenoxuron	156.13	1.036	0.9971	0–1	79.326	4.7620	0.7626
Clorfluazuron	153.56	1.076	0.9907	0–1	81.309	4.7572	0.8002
Teflubenzuron	155.74	0.828	0.9985	0–1	76.122	4.9030	0.8288
Lufenuron	154.81	1.056	0.9963	0–1	81.081	4.9497	0.7936

Table 8 Adsorption isotherm constants for BUs adsorption on HBPS-COOH

T = 303 K	Langmuir isotherm model				Freundlich isotherm model		
	q_{max} (mg g^{-1})	K_L	R^2	R_L	K_F (mg$^{1-1/n}$ L$^{1/n}$ g^{-1})	n	R^2
Diflubenzuron	100.62	1.068	0.9939	0–1	53.987	4.1549	0.7622
Hexaflumuron	92.63	1.014	0.9923	0–1	51.260	4.8152	0.8657
Flufenoxuron	82.99	1.064	0.9906	0–1	54.721	4.5176	0.8362
Clorfluazuron	94.43	0.952	0.9916	0–1	46.671	4.6576	0.7568
Teflubenzuron	96.24	0.992	0.9925	0–1	46.579	4.4624	0.8360
Lufenuron	92.17	0.968	0.9961	0–1	45.782	4.8544	0.7874

Table 9 Adsorption isotherm constants for BUs adsorption on HBPS-C_6H_{13}

$T = 303$ K	Langmuir isotherm model				Freundlich isotherm model		
	q_{max} (mg g^{-1})	K_L	R^2	R_L	K_F (mg$^{1-1/n}$ L$^{1/n}$ g^{-1})	n	R^2
Diflubenzuron	87.50	0.968	0.9963	0–1	44.071	4.4716	0.8314
Hexaflumuron	82.12	0.932	0.9949	0–1	40.737	4.6980	0.8517
Flufenoxuron	85.92	1.144	0.9926	0–1	51.487	4.1232	0.7956
Clorfluazuron	85.99	0.844	0.9965	0–1	49.820	4.9324	0.8604
Teflubenzuron	87.86	1.207	0.9982	0–1	56.294	4.9292	0.7621
Lufenuron	84.83	1.160	0.9988	0–1	49.910	4.8564	0.8904

Table 10 Adsorption isotherm constants for BUs adsorption on HBPS-β-CD

$T = 303$ K	Langmuir isotherm model				Freundlich isotherm model		
	q_{max} (mg g^{-1})	K_L	R^2	R_L	K_F (mg$^{1-1/n}$ L$^{1/n}$ g^{-1})	n	R^2
Diflubenzuron	127.12	1.096	0.9989	0–1	76.757	4.2768	0.8749
Hexaflumuron	111.44	1.148	0.9975	0–1	65.916	4.4928	0.7813
Flufenoxuron	123.59	0.828	0.9987	0–1	74.393	4.8972	0.8314
Clorfluazuron	120.44	1.088	0.9953	0–1	65.399	4.7032	0.7298
Teflubenzuron	125.73	0.849	0.9951	0–1	74.878	4.8156	0.8725
Lufenuron	110.75	1.057	0.9998	0–1	65.061	4.7536	0.8779

Table 11 Adsorption isotherm constants for BUs adsorption on HBPS-Ph

$T = 303$ K	Langmuir isotherm model				Freundlich isotherm model		
	q_{max} (mg g^{-1})	K_L	R^2	R_L	K_F (mg$^{1-1/n}$ L$^{1/n}$ g^{-1})	n	R^2
Diflubenzuron	101.83	1.072	0.9905	0–1	53.046	4.1526	0.7788
Hexaflumuron	87.23	1.417	0.9956	0–1	54.683	4.7532	0.8583
Flufenoxuron	90.92	1.064	0.9941	0–1	60.361	4.9976	0.8326
Clorfluazuron	94.73	0.856	0.9956	0–1	62.791	4.8816	0.7929
Teflubenzuron	92.14	1.148	0.9967	0–1	54.808	4.8756	0.8077
Lufenuron	95.75	0.916	0.9944	0–1	49.645	4.9775	0.8266

7–11 show the values of parameters calculated by the Langmuir and Freundlich isotherms. The comparison of correlation coefficients (R^2) of the linearized form of both equations indicates that the Langmuir model adequately described the adsorption of BUs on the adsorbent.

4. Conclusions

In this study, a series of HBPS materials with different end groups were designed and prepared. The materials were applied to the adsorption of BUs and the methods for the determination of adsorption kinetics and adsorption isotherms and quantum mechanical calculations were studied. In this research, the lowest energy stable configuration and the binding energy in different binding configurations were determined. Based on the calculated binding energy, the adsorption mechanism under different binding configurations was analyzed. At the same time, the adsorption kinetics and thermodynamic mechanism

of the adsorbent were studied. The adsorption kinetic model was fitted and verified by the quantum chemical results. The BUs adsorption represented by diflubenzuron was discussed. The ability of the insecticide to bind to different terminal functional groups on the hyperbranched polymer structure and the binding mechanism were evaluated. In the future research, the method can be used to calculate and screen the target analyte and the selected adsorbent first, and then study the adsorption effect on the basis of the screening results, which can greatly improve the experimental efficiency. Furthermore, the database of the lowest energy binding configuration between the adsorbent and the analyte can be established under the conditions, which provides convenience for the high-throughput screening of adsorbents.

Conflicts of interest

The authors have declared no conflict of interest.

Acknowledgements

References

1 M. D. Gil-García, M. Martínez-Galera, T. López-López, J. L. Martínez-Vidal, M. C. Mahedero and F. Salinas, *Talanta*, 2001, **53**, 915–925.

2 F. Matsumura, *Pestic. Biochem. Physiol.*, 2010, **97**, 133–139.

3 M. D. Gil García, M. Martínez Galera, D. Barranco Martínez and J. Gisbert Gallego, *J. Chromatogr. A*, 2006, **1103**, 271–277.

4 EU Pesticides database, 2018, available online, http://ec.europa.eu/food/plant/pesticides/eu-pesticides-database/public/?event=homepage&language=EN, accessed, September 25, 2019.

5 Z. Żołek-Tryznowska and J. Izdebska, *Compos. Interfaces*, 2012, **19**, 441–451.

6 P. B. Pirozhnikov, I. V. Korolev, N. G. Kuzina and L. N. Mashlyakovskii, *Russ. J. Appl. Chem.*, 2013, **86**, 1549–1562.

7 Y. K. Jeong, T.-w. Kwon, I. Lee, T.-S. Kim, A. Coskun and J. W. Choi, *Nano Lett.*, 2014, **14**, 864–870.

8 X. Chen, S. G. Parker, G. Zou, W. Su and Q. Zhang, *ACS Nano*, 2010, **4**, 6387–6394.

9 C. Aydogan, G. Yilmaz and Y. Yagci, *Macromolecules*, 2017, **50**, 9115–9120.

10 H. Wang, Z. Wang, R. Yue, F. Gao, R. Ren, J. Wei, X. Wang and Z. Kong, *J. Hazard. Mater.*, 2020, **384**, 121288.

11 S. Grimme, *J. Comput. Chem.*, 2004, **25**, 1463–1473.

12 S. Grimme, S. Ehrlich and L. Goerigk, *J. Comput. Chem.*, 2011, **32**, 1456–1465.

13 U. Domańska and Z. Żołek-Tryznowska, *J. Chem. Thermodyn.*, 2009, **41**, 821–828.

14 X. Wu, M. C. Vargas, S. Nayak, V. Lotrich and G. Scoles, *J. Chem. Phys.*, 2001, **115**, 8748–8757.

15 T. Mueller and G. Ceder, *J. Phys. Chem. B*, 2005, **109**, 17974–17983.

16 J. Pang, Y. Liao, X. Huang, Z. Ye and D. Yuan, *Talanta*, 2019, **199**, 499–506.

17 C. Gao and D. Yan, *Prog. Polym. Sci.*, 2004, **29**, 183–275.

18 D. Muscat and R. A. T. M. van Benthem, in *Dendrimers III: Design, Dimension, Function*, ed. F. Vögtle, Springer Berlin Heidelberg, Berlin, Heidelberg, 2001, pp. 41–80.

19 G. M. Dykes, *J. Chem. Technol. Biotechnol.*, 2001, **76**, 903–918.

20 H. Wang, Q. Xu, J. Wang, W. Du, F. Liu and X. Hu, *Biosens. Bioelectron.*, 2018, **100**, 105–114.

21 L. Chen, Q. Wang, R. Huang, C. Mao, J. Shang and F. Bi, *J. Agric. Food Chem.*, 2005, **53**, 38–41.

22 W. Lu, J. Li, Y. Sheng, X. Zhang, J. You and L. Chen, *J. Colloid Interface Sci.*, 2017, **505**, 1134–1146.

23 H. Liu, K. Tian, J. Ning, Y. Zhong and Y. Hu, *ACS Catal.*, 2019, **9**, 1211–1219.

24 J. Li, R. Dong, X. Wang, H. Xiong, S. Xu, D. Shen, X. Song and L. Chen, *RSC Adv.*, 2015, **5**, 10611–10618.

25 G. Wu, J. Ma, S. Li, J. Guan, B. Jiang, L. Wang, J. Li, X. Wang and L. Chen, *J. Colloid Interface Sci.*, 2018, **528**, 360–371.

26 H. Zhang, C. Guo, J. Ren, J. Ning, Y. Zhong, Z. Zhang and Y. Hu, *Chem. Commun.*, 2019, **55**, 14050–14053.

27 X. Cai, J. Li, Z. Zhang, F. Yang, R. Dong and L. Chen, *ACS Appl. Mater. Interfaces*, 2014, **6**, 305–313.

28 Q. Kong, J. Wei, Y. Hu and C. Wei, *J. Hazard. Mater.*, 2019, **363**, 161–169.

29 Y. Wu, E. Hu, W. Dai, Z. Li, Y. Zhong and Y. Hu, *RSC Adv.*, 2017, **7**, 5093.

30 G. Wu, J. Ma, S. Li, S. Wang, B. Jiang, S. Luo, J. Li, X. Wang, Y. Guan and L. Chen, *Environ. Res.*, 2020, **186**, 109542.

31 G. Wu, J. Ma, S. Wang, H. Chai, L. Guo, J. Li, A. Ostovan, Y. Guan and L. Chen, *J. Hazard. Mater.*, 2020, **394**, 122556.

32 H. Wang, L. Hu, W. Li, R. Lu, S. Zhang, W. Zhou and H. Gao, *J. Chromatogr. A*, 2016, **1471**, 60–67.